NREL
NATIONAL RENEWABLE ENERGY LABORATORY

A Comparative Study of the Defect Point Physics and Luminescence of the Kesterites Cu_2ZnSnS_4 and $Cu_2ZnSnSe_4$ and Chalcopyrite $Cu(In,Ga)Se_2$

Preprint

Manuel J. Romero, Ingrid Repins, Glenn Teeter, Miguel A. Contreras, Mowafak Al-Jassim, and Rommel Noufi

Presented at the 2012 IEEE Photovoltaic Specialists Conference
Austin, Texas
June 3–8, 2012

Conference Paper
NREL/CP-5200-54140
August 2012

Contract No. DE-AC36-08GO28308

NOTICE

Available electronically at http://www.osti.gov/bridge

Available for a processing fee to U.S. Department of Energy
and its contractors, in paper, from:

U.S. Department of Energy
Office of Scientific and Technical Information

P.O. Box 62
Oak Ridge, TN 37831-0062
phone: 865.576.8401
fax: 865.576.5728
email: mailto:reports@adonis.osti.gov

Available for sale to the public, in paper, from:

U.S. Department of Commerce
National Technical Information Service
5285 Port Royal Road
Springfield, VA 22161
phone: 800.553.6847
fax: 703.605.6900
email: orders@ntis.fedworld.gov
online ordering: http://www.ntis.gov/help/ordermethods.aspx

Cover Photos: (left to right) PIX 16416, PIX 17423, PIX 16560, PIX 17613, PIX 17436, PIX 17721

Printed on paper containing at least 50% wastepaper, including 10% post consumer waste.

A Comparative Study of the Defect Point Physics and Luminescence of the Kesterites Cu_2ZnSnS_4 and $Cu_2ZnSnSe_4$ and Chalcopyrite $Cu(In,Ga)Se_2$

Manuel J. Romero, Ingrid Repins, Glenn Teeter, Miguel A. Contreras, Mowafak Al-Jassim, Rommel Noufi

National Renewable Energy Laboratory, Golden, CO 80401 USA

***Abstract* — In this contribution, we present a comparative study of the luminescence of the kesterites Cu_2ZnSnS_4 (CZTS) and $Cu_2ZnSnSe_4$ (CZTSe) and their related chalcopyrite $Cu(In,Ga)Se_2$ (CIGSe). Luminescence spectroscopy suggests that the electronic properties of Zn-rich, Cu-poor kesterites (both CZTS and CZTSe) and Cu-poor CIGSe are dictated by fluctuations of the electrostatic and chemical potentials. The large redshift in the luminescence of grain boundaries in CIGSe, associated with the formation of a neutral barrier is clearly observed in CZTSe, and, to some extent, in CZTS. Kesterites can therefore replicate the fundamental electronic properties of CIGSe.**

***Index Terms* — chalcopyrite, kesterite, thin film, cathodoluminescence.**

I. Introduction

The kesterites Cu_2ZnSnS_4 (CZTS) and $Cu_2ZnSnSe_4$ (CZTSe) are attracting considerable interest because first principles calculations predict that their electronic properties must be similar to their associated chalcopyrite $Cu(In,Ga)Se_2$ (CIGSe) compounds [1,2]. Kesterite-based solar cells can therefore potentially achieve the high conversion efficiencies demonstrated by chalcopyrites (> 20%) [3] while covering the demand in a projected TeraWatt-scale photovoltaic (PV) scenario in which the relative scarcity of indium and the competition for this resource with other manufacturing sectors will limit the expansion of CIGSe-based PV [4,5].

The electronic structure of Cu-poor CIGSe is dominated by the formation of copper vacancies (V_{Cu}) and the stabilization of defect complexes with low formation energies ($2V_{Cu}^{-} + In_{Cu}^{2+}$) [6,7]. The high densities of shallow donor and acceptor levels lead to the delocalization of their associated electronic states and introduces local variations in the chemical and electrostatic potentials as revealed by luminescence spectroscopy [8, 9]. In chalcopyrites, these local variations of the chemical potential are accommodated by the spontaneous segregation of α-like and (copper-deficient) β-like domains (named after the α and β phases of the phase diagram) in the nanometer scale [10, 11]. This nanoscale morphology is regarded as beneficial to the efficiency of the solar cell because electrons and holes will dissociate respectively into electron-donor (α) and electron-acceptor (β) domains and then diffuse to the appropriate electrode within the α or β phase (hence reducing recombination).

Another critical aspect to be considered is the electronic properties of grain boundaries. In Cu-poor CIGSe, grain boundaries develop a *neutral barrier* for holes that do not otherwise impede the electron transport and reduce recombination [12,13]. The formation of this neutral barrier is largely responsible for the benign behavior of grain boundaries [14] and critical to achieving high conversion efficiencies.

In this contribution, luminescence spectroscopy and spectrum imaging [15] measurements are applied to Zn-rich, Cu-poor kesterite thin films and the results are compared to Cu-poor CIGSe. The electronic structure of grain boundaries in the kesterite is investigated by luminescence microscopy and the results compared to those from Cu-poor CIGSe obtained by NREL's three-stage process [16].

II. Experimental

CZTS thin films are obtained by coevaporation of Cu, Zn, and Sn from three independent effusion cells under a molecular beam of S_2 supplied by a valved-cracking source. The molybdenum-coated glass substrates are actively heated to 470 ºC. The base pressure of the chamber is 8.0×10^{-6} Torr, rising to 1.7×10^{-4} Torr during the deposition. More details, including information on the elemental sources, can be found in reference 17. The stoichiometry of the films used in this study is confined to the region of stability for the kesterite phase and slightly displaced towards the ZnS-SnS_2 boundary of the phase diagram. These CZTS films are therefore Cu-poor (Cu/(Zn+Sn) ~ 0.74) and Zn-rich (Zn/Sn ~ 1.36), which is consistent with the stoichiometry of the best CZTS solar cells reported in the literature [18,19].

CZTSe thin films are obtained by coevaporation from elemental sources. The molybdenum-coated glass substrates are actively heated to 470-500 ºC. In a two-stage process, Cu and Zn are first supplied under an overpressure of Sn and Se to form the Cu-rich (Cu/(Zn+Sn) > 1) kesterite with copper selenide as a secondary phase. During the second stage, the Cu source is shut off and the deposition proceeds to form Zn-rich ((Zn/Sn = 1.15) and Cu-poor (Cu/(Zn+Sn) = 0.86) CZTSe. Similarly to the three-stage process for CIGSe, the two-stage process for CZTSe revolves around the formation of excess copper selenide and the accompanying emissivity signature that can be monitored during deposition. More details can be found in reference 20.

These films are compared to NREL's high efficiency CIGSe, with the standard Cu/(In+Ga) ratio ~ 0.9 and Ga/(In+Ga) ~ 0.3, as required for record performance [21].

III. Luminescence Spectroscopy

The fundamental aspects of the recombination in these coevaporated Zn-rich, Cu-poor kesterites are first investigated by luminescence spectroscopy and the results compared to those previously obtained in Cu-poor chalcopyrites. The influence of the excitation density (measured by the electron-beam current I_b[22]) on the emission spectrum at cryogenic temperatures (T = 15 K) for CIGSe is shown in Fig. 1a. These measurements are complemented by the influence of the temperature (ΔT = 20-300 K) –Fig. 1b. The spectrum consists of a broadband luminescence centered at few hundreds of milielectronvolts (meV) below the bandgap E_g. The emission spectrum shows a pronounced *blueshift* with excitation density (~40 meV over three decades of excitation density) and a *blueshift* with temperature (~50 meV from T = 300 K down to T = 20 K).

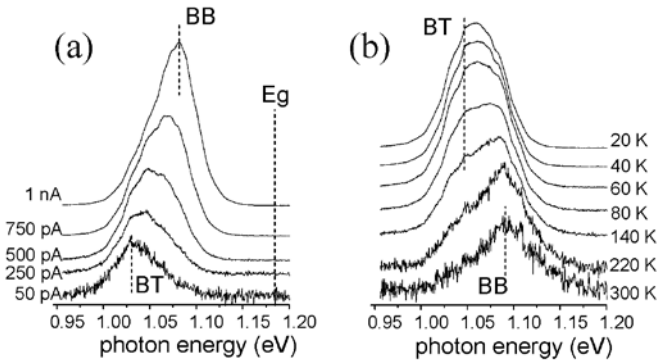

Fig. 1. Influence of the excitation density (measured by the electron-beam current I_b) on the emission spectrum of Cu-poor CIGSe at cryogenic temperatures (T = 15 K). Influence of the temperature (T= 20-300 K) at I_b = 500 pA.

The luminescence of Cu-poor CIGSe has been extensively investigated by other authors [8, 9] and here we summarize the aspects most relevant to our comparative study of chalcopyrites and kesterites. This is better described by first considering the point defect structure of chalcopyrites under Cu deficiency. From first principles calculations [23], the dominant donors and acceptors are, respectively, the indium-on-copper-antisite (In_{Cu}) (stabilized through the formation of ($2V_{Cu}^{-} + In_{Cu}^{2+}$) defect complexes) and the copper vacancy (V_{Cu}). The prevalence of these intrinsic point defects in the chalcopyrite structure leads to the delocalization of the donor and acceptor states and the formation of bands. In this scenario of high density of intrinsic point defects and compensation, local deviations in the distribution of donors (+) and acceptors (–) will introduce potential fluctuations in the band structure [24]. The schematics of the band diagram (including these potential fluctuations) are shown in Fig. 2. Using this representation, the luminescence includes two emission bands: one associated to the band tails of the donor and acceptor bands (BT)—which follow the potential fluctuations—and the other to transitions between the donor and acceptor bands (BB) [9], as shown schematically in Fig. 2.

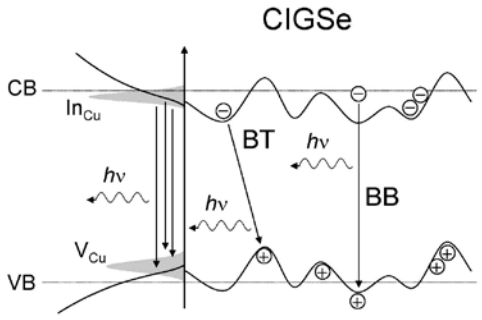

Fig. 2. Schematics of the band diagram for Cu-poor CIGSe. The luminescence is dominated by band-tail (BT) and band-to-band (BB) transitions between delocalized donor and acceptor states. Local deviations in the distribution of donors and acceptors lead to potential fluctuations.

At low temperature *and* low excitation density (I_b = 50 pA in Fig. 1a), the spectrum is dominated by band-tail transitions corresponding to the lowest energy states in the landscape of potential fluctuations. The *blueshift* with the excitation density at low temperature results from the reduction of the amplitude of the potential fluctuations leading to an increase in the transition energy (towards BB, I_b = 1 nA in Fig. 1a). In our case, we observe a saturation of the transition energy at high excitation densities (I_b > 1 nA) below the measured bandgap [25]. This suggests that (quasi)-free electron-to-acceptor band transitions (associated with the V_{Cu}) are dominant at high excitation densities ($\Delta n,p > 10^{17}$ cm^{-3}) with no contribution of the excitonic transitions observed in near stoichiometric chalcopyrites [26]. The overall *blueshift* with temperature (Fig. 1b) is a direct consequence of the thermal excitation of electrons (holes) from the band-tail states to the donor (acceptor) band—resulting in the quenching of the BT transition observed at moderate excitation densities I_b = 500 pA, Fig. 1b. It also results in the increase in the energy of free electrons (holes) in the donor (acceptor) bands with further increasing temperature—resulting in the blueshift of the BB transition.

Similar spectroscopy measurements in Zn-rich, Cu-poor kesterites reveal a near one-to-one correspondence with Cu-poor CIGSe (Fig. 3). The spectrum also consists of BT and BB emission bands with similar excitation density and temperature dependencies (not shown) to those observed in

chalcopyrites. There is a dramatic loss of quantum efficiency of the luminescence of the CZTS when compared to CIGSe (0.02 to 1), which improves significantly for CZTSe but remains well below than that of CIGSe (0.2 to 1).

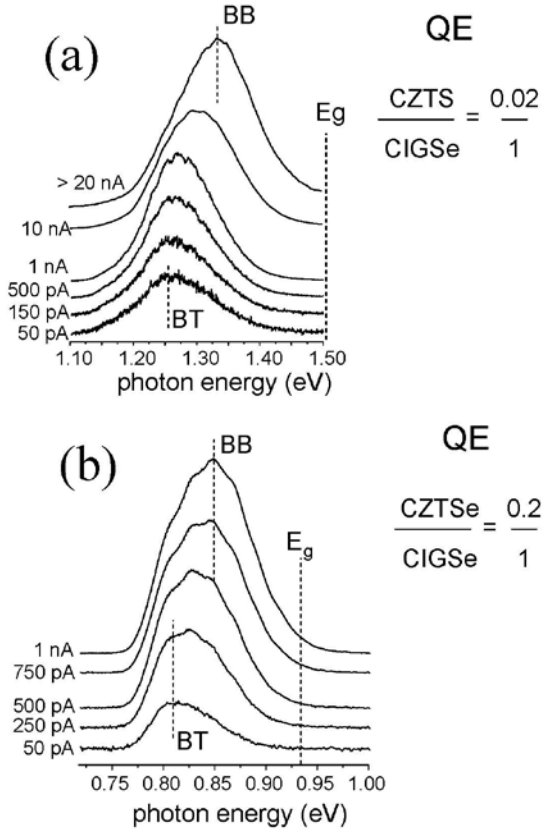

Fig. 3. Influence of the excitation density (measured by the electron-beam current I_b) on the emission spectrum of Zn-rich, Cu-poor CZTS and CZTSe at cryogenic temperatures (T = 15 K).

In the coevaporated CZTS, the high recombination led by antisite substitutions between the cations Cu(I), Zn(II), and Sn(IV), sulfur vacancies (V_S) and their associated electronic levels deep inside the bandgap [2] overruns the prospective beneficial effects of the potential fluctuations. Because of the high contribution of nonradiative recombination, it is very difficult to extract information on the amplitude and length scale of these fluctuations.

In the coevaporated CZTSe, on the other hand, the blueshift with the excitation density at cryogenic temperatures is estimated in ~40 meV over three decades of excitation density (to transition from BT to BB), and saturates at $I_b \sim 2$ nA with BB at ~100 meV below the estimated bandgap. These are very similar values to those obtained from CIGSe, suggesting that the amplitude and length scale of the fluctuations of the electrostatic potential are comparable in both kesterite and chalcopyrite selenides (see Fig. 4). Indeed, similar transition energy at saturation (relative to the bandgap) points toward a large number of Cu vacancies for both CIGSe and CZTSe: the V_{Cu}-acceptor state has similar shallow levels at $\varepsilon(-/0) = 0.02$ eV in CZTSe and $\varepsilon(-/0) = 0.03$ eV in CIGSe. Although these measurements suggest that the copper vacancies are primarily involved in the band-to-band transitions in CZTSe, it is likely that the deeper acceptor level at $\varepsilon(-/0) = 0.12$ eV associated with copper-on-zinc antisites (Cu_{Zn})—the most energetically favorable point defect in CZTS(e)—also participates in the formation of the acceptor band, even under Cu-poor, Zn-rich conditions.

To reproduce the fluctuations, the formation of neutral ($2V_{Cu}^{-} + Zn_{Cu}^{2+}$) defect complexes to accommodate the large number of Cu vacancies in the kesterite structure (under Zn-rich conditions) might parallel that of the ($2V_{Cu}^{-} + Cu_{In}^{2+}$) in chalcopyrites [2].

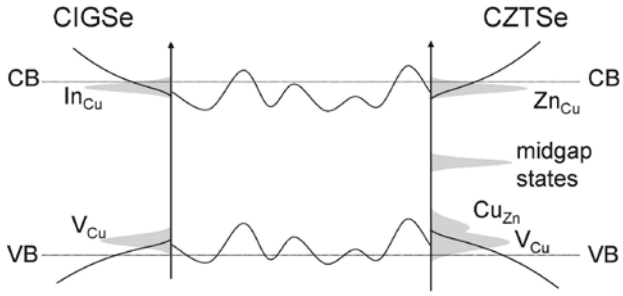

Fig. 4. Schematics of the band diagram for Cu-poor CIGSe and Cu-poor, Zn-rich CZTSe. Based on the results of the luminescence spectroscopy measurements, the amplitude and length scale of the potential fluctuations should be similar in CIGSe and CZTSe.

All these results suggest that the electronic properties of Zn-rich, Cu-poor kesterites (both CZTS and CZTSe) and Cu-poor CIGSe are dictated by fluctuations of the electrostatic and chemical potentials. From the increase in the efficiency of the luminescence (CZTSe vs. CZTS), the density of midgap states is largely mitigated in the selenide and, consequently, the point defect structure of CZTSe becomes more closely related to that of CIGSe.

IV. Grain Boundary Luminescence

In Section III, we have shown evidence that (for the coevaporation route) the point defect physics of Zn-rich, Cu-poor CZTSe and Cu-poor CIGSe are closely related, with Zn-rich, Cu-poor CZTS being somehow related. Along with the point defect physics, another critical aspect of the electronic properties in Cu-poor CIGSe is the benign behavior of grain boundaries [14]. The leading explanation is based on the formation of a large neutral barrier for holes that do not otherwise impede the electron transport and reduce recombination [12]. The existence of this neutral barrier has been confirmed experimentally by several methods [13,27].

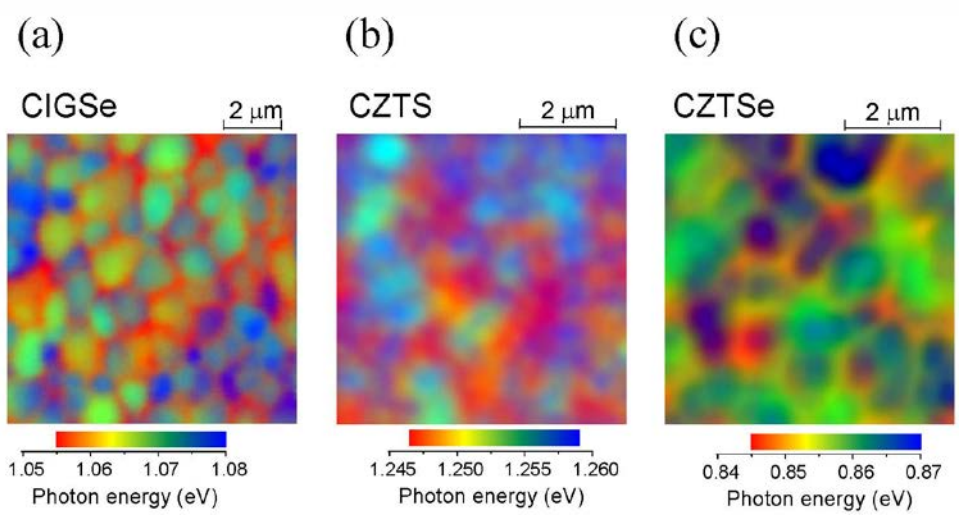

Fig. 5. Spectrum imaging measurements of the luminescence. (a) A representative map of the photon energy of the luminescence from CIGSe thin films used in PV applications. A redshift of the emission spectrum (10 to 15 meV) is observed at grain boundaries. Similar maps of the transition energy for CZTS (b) and CZTSe (c). The spatial variation in the emission spectrum of CZTS is mostly a result of grain-to-grain inhomogeneity. The characteristic redshift at grain boundaries is more clearly seen in CZTSe.

Among these methods, luminescence reveals a *redshift* of the emission spectrum at grain boundaries in CIGSe consistent with the incorporation of V_{Cu} acceptors to the boundary, as predicted by the neutral barrier model.

Fig. 5a shows a map of the photon energy of the luminescence from CIGSe (color coded so that red and blueshifts in the emission spectrum are intuitive [29]). We observe a 10 to 15 meV redshift of the luminescence at grain boundaries when compared to the grain interiors. This is consistent with the copper depletion observed at grain boundaries by atom probe tomography [30]: the incorporation of V_{Cu}-acceptor states will extend the acceptor band into the gap, hence the observed redshift. We have firmly established that this redshift is absolutely critical in achieving high efficiency in CIGSe and must be related to the formation of the neutral barrier.

In the kesterites, the redshift at the grain boundaries is not clearly seen for CZTS (see Fig. 5b), and the spatial variation in the emission spectrum is largely dominated by grain-to-grain inhomogeneity. The redshift at grain boundaries, when present, is much less pronounced (only 2-4 meV). In the CZTSe, on the other hand, we can clearly observe this redshift at the grain boundaries (see Fig. 5c). We are finding grain boundaries in CZTSe where the magnitude of the redshift is par with that of the grain boundaries of CIGSe (10-15 meV). This is an extremely important result suggesting that the kesterite can duplicate the electronic structure of the grain boundaries found in chalcopyrites, possibly because of similar atomistic configuration and point defect structure. Unfortunately not all boundaries show this effect, in contrast to CIGSe where this redshift is commonplace. The higher degree of cation disorder of the kesterite structure—induced by substitutions among the cations Cu(I), Zn(II), and Sn(IV) — can account for the variability in the defect point structure of grain boundaries and their luminescence.

V. Summary and Conclusions

We have found that the point defect luminescence of Zn-rich, Cu-poor CZTSe and Cu-poor CIGSe are closely related, with Zn-rich, Cu-poor CZTS being somehow related. The results of the spectroscopy measurements are consistent with high densities of intrinsic point defects with donor and acceptor character leading to fluctuations of the electrostatic and chemical potentials.

Not only does Zn-rich, Cu-poor CZTSe mimic very exclusive aspects of the point defect luminescence of Cu-poor CIGSe, but the grain boundaries of the kesterite can replicate the luminescence observed in chalcopyrites, in agreement with the neutral barrier model. This is an extremely important result, as the formation of this neutral barrier is largely responsible for the benign behavior of grain boundaries and obviously critical to achieving high conversion efficiencies.

In conclusion, for these films obtained by coevaporation, the recombination processes operating in Zn-rich, Cu-poor CZTSe are closely related to its relative Cu-poor CIGSe and the similarities between the kesterite and chalcopyrite selenides are more pronounced than in the case of the kesterite sulfide. As a result, current conversion efficiencies for CZTSe solar cells at NREL are higher than those of CZTS. Moving forward to higher efficiencies will require a reduction of the variability in the point defect structure within grain interiors and particularly among the grain boundaries of CZTSe.

ACKNOWLEDGEMENTS

This work was supported by the U.S. Department of Energy under Contract No. DE-AC36-08-GO28308 with the National Renewable Energy Laboratory.

REFERENCES

[1]. A. Nagoya and R. Asahi, Phys. Rev. B **81**, 113202 (2010).
[2]. S. Chen, J.-H. Yang, X. G. Gong, A. Walsh, and S.-H. Wei, Phys. Rev. B **81**, 245204 (2010).
[3]. P. Jackson, D. Hariskos, E. Lotter, S. Paetel, R. Wuerz, R. Menner, W. Wischmann, and M. Powalla, Progress in Photovoltaics: Research and Applications (2011). Published Online: DOI: 10.1002.
[4]. B. A. Andersson, Progress in Photovoltaics: Research and Applications **8**, 61 (2000).
[5]. A. Feltrin and A. Freundlich, Renewable Energy 33, 180 (2008).
[6]. S. B. Zhang, S.-H. Wei, and A. Zunger, Phys. Rev. Lett. **78**, 4059 (1997); S. B. Zhang, S.-H. Wei, A. Zunger, and H. Katayama-Yoshida, Phys. Rev. B **57**, 9642 (1998).
[7]. S.-H. Wei, S. B. Zhang, and A. Zunger, Appl. Phys. Lett. **72**, 3199 (1998).
[8]. I. Dirnstorfer, M. Wagner, D. M. Hofmann, M. D. Lampert, F. Karg, and B. K. Meyer, Phys. Status Solidi A **168**, 163(1998).
[9]. J. Krustok, H. Collan, M. Yakushev, and K. Hjelt, Physica Scripta. T**79**, 179 (1999).
[10]. B. J. Stanbery, Proceedings of the 31st IEEE Photovoltaics Specialist Conference, IEEE, New York, 2005, p. 355.
[11]. Y. Yan, R. Noufi, K. M. Jones, K. Ramanathan, M. M. Al-Jassim, and B. J. Stanbery, Appl. Phys. Lett. **87**, 121904 (2005).
[12]. C. Persson and A. Zunger, Phys. Rev. Lett. **91**, 266401 (2003); C. Persson and A. Zunger, Appl. Phys. Lett. **87**, 211904 (2005).
[13]. M. Hafemeister, S. Siebentritt, J. Albert, M. Ch. Lux-Steiner, and S. Sadewasser, Phys. Rev. Lett. **104**, 196602 (2010).
[14]. Y. Yan, C.-S. Jiang, R. Noufi, Su-Huai Wei, H. R. Moutinho, and M. M. Al-Jassim, Phys. Rev. Lett. **99**, 235504 (2007).
[15]. D. Abou-Ras, M. Nichterwitz, M. J. Romero, and S. S. Schmidt. Electron Microscopy of Thin Films for Solar Cells; in Handbook of Advanced Characterization Techniques for Thin Film Solar Cells. Ed. Wiley-VCH 2011. ISBN: 978-3-527-41003-3.
[16]. M. A. Contreras, I. Repins, W. K. Metzger, M. J. Romero, D. Abou-Ras. Physica Status Solidi **206**, 1876 (2009).
[17]. G. Teeter, H. Du, J. E. Leisch, M. Young, F. Yan, S. W. Johnston, P. Dippo, D. Kuciauskas, M. J. Romero, P. Newhouse, S. E. Asher, and D. S. Ginley, in Proceedings of the 35th Photovoltaic Specialists Conference, 650 (2010).
[18]. T. K. Todorov, K. B. Reuter, and D. B. Mitzi Advanced Materials **22**, 1 (2010)
[19]. K. Wang, O. Gunawan, T. Todorov, B. Shin, S. J. Chey, N. A. Bojarczuk, D. Mitzi, and S. Guha, Appl. Phys. Lett. **97**, 143508 (2010).
[20]. I. Repins, C. Beall, N. Vora, C. DeHart, D. Kuciauskas, P. Dippo, B. To, J. Mann, W.-C. Hsu, A. Goodrich, and R. Noufi, Solar Energy Materials and Solar Cells (2012). doi: 10.1016/j.somat.202.01.008.
[21]. M. A. Contreras, M. J. Romero, and R. Noufi, Thin Solid Films **511-512**, 51 (2006).
[22]. As a rule of thumb, an electron-beam current of I_b = 1 nA corresponds to an excess carrier density of $\Delta n,p \sim 1017$ cm-3.
[23]. T. Maeda, T. Wada, J. Phys. Chem. Solids **66**, 1924 (2005).
[24]. B.I. Shklovskii and A.L. Efros, Electronic Properties of Doped Semiconductors (Springer, Berlin, 1984).
[25]. The bandgap is measured by quantum efficiency measurements.
[26]. N. Rega, S. Siebentritt, J. Albert, S. Nishiwaki, A. Zajogin, M.Ch. Lux-Steiner, R. Kniese, and M.J. Romero, Thin Solid Films **480-481**, 286 (2005).
[27]. C.-S. Jiang, R. Noufi, J. A. AbuShama, K. Ramanathan, H. R. Moutinho, J. Pankow, and M. M. Al-Jassim, Appl. Phys. Lett. **84**, 3477 (2004)
[28]. M.J. Romero, C.-S. Jiang, R. Noufi, and M. Al-Jassim, Appl. Phys. Lett. **87**, 172106 (2005).
[29]. The photon energy map is generated by first defining the region of interest on the emission spectrum (for example, 0.8 eV to 1.1 eV), which is then divided in three different channels (Red, 0.8 eV to 0.9 eV; Green: 0.9 eV to 1.0 eV; Blue: 1.0 eV to 1.1 eV). The total counts in each channel are normalized to the 0-255 scale of the RGB code to generate the color of each pixel.
[30]. O. Cojocaru-Mirédin, P.-P. Choi, D. Abou-Ras, D. Raabe in Proceedings of the 37th IEEE Photovoltaic Specialists Conference, Seattle, WA, June 19-24 (2011).